SPECTRUM OF ENGINEERING SCIENCES
ISSN (E) 3007-3138 (P) 3007-312X Volume 4, Issue 3, 2026

Multiscale 3D CFD Transport and Interfacial Wetting Dynamics in Membrane Contactors for Ionic Liquid-Based Post-Combustion CO2 Capture

Dr. Imran khan Swati*, Sameer khan
Department of Chemical Engineering, university of engineering and technology peshawar pakistan-Email: imranswati@uetpeshawar.edu.pk, ORCID Id : 0009-0008-6314-1392
Department of Chemical engineering, University of Engineering and Technology, Peshawar Pakistan-24pwche1782@uetpeshawar.edu.pk, ORCID Id: 0009-0005-6919-9470

DOI:https://doi.org/10.5281/zenodo.24053150

Keywords
CFD, Membrane Contactor, CO2 Capture, Ionic Liquid ([OMIM][BF4]), Mass Transfer, Pore Wetting, Sweep Ratio, Packing Density.

Article History
Received on 20 Jan 2026
Accepted on 20, march 2026
Published on 27 March 2026

Copyright @Author
Corresponding Author

Dr. Imran khan Swati*

Post-combustion carbon dioxide capture using membrane contactors offers exceptional interfacial area without direct phase dispersion, yet localized concentration polarization, boundary layer mass transfer resistance, and module design trade-offs present critical scale-up challenges. This study presents an advanced 3D Computational Fluid Dynamics (CFD) investigation of non-dispersive CO2 absorption from a binary gas feed (15 vol% CO2 / 85 vol% N2) into a continuously recirculated 50 vol% aqueous ionic liquid solution ([OMIM][BF4]) across a hydrophobic flat-sheet PTFE membrane module under counter-current flow conditions. By resolving conjugated convective and diffusive species transport equations, the numerical model captures the spatial evolution of species concentration profiles and directional flux behavior. Results reveal a distinct transport dichotomy: convective flux dominates along the axial direction but declines progressively from module inlet to outlet as the ionic liquid nears saturation, diminishing the local concentration driving force. Conversely, radial diffusive flux intensifies across the membrane boundary layer due to localized concentration polarization at the gas-liquid interface within the pore structure. Parametric evaluation of the liquid sweep ratio demonstrates a strong non-linear enhancement in separation efficiency, with CO2 removal increasing from 38% at a sweep ratio of 0.5 to 95% at a ratio of 3.0, albeit at the expense of higher solvent inventory and regeneration duties. Furthermore, module geometry optimization highlights that extending effective module length enhances residence time and overall capture efficiency, but elevates axial pressure drops and risks exceeding the Liquid Entry Pressure (LEP) threshold, leading to pore wetting. Increasing packing density—scaling fiber count from 5,000 to over 40,000—successfully bypasses pressure-induced wetting limits by increasing mass transfer surface area, achieving over 90% CO2 capture. This multiscale CFD framework directly links microscopic transport

mechanisms to module-scale hydrodynamics, providing quantitative design criteria for intensified ionic liquid-based carbon capture processes

1. INTRODUCTION:

Carbon dioxide emissions generated from burning fossil fuels are the primary driver of global climate change and atmospheric degradation. To reduce the impact of these industrial flue gases from power plants, cement factories, and steel manufacturing facilities, post-combustion carbon capture has become a critical operational strategy [1]. The conventional approach relies on chemical absorption towers filled with liquid amine solutions. While these traditional towers are widely used, they suffer from severe operational problems. They require massive amounts of thermal energy to strip the captured carbon dioxide and reuse the liquid, the amine chemicals easily evaporate and degrade over time, equipment corrodes rapidly, and the liquids frequently foam, flood, or overflow inside the large absorption columns [2].

Membrane contactors provide a much cleaner and more efficient alternative to conventional towers. In a membrane contactor, a hydrophobic porous membrane acts as a static physical wall that keeps the flowing gas stream and the liquid absorbent completely separated. Instead of forcefully mixing the gas and liquid together, carbon dioxide naturally diffuses through the microscopic gas-filled pores of the membrane wall and dissolves into the liquid flowing on the other side. This specialized design packs a huge interfacial contact area into a very small equipment footprint, allows independent control of both gas and liquid flow speeds, and completely eliminates common operational issues like liquid entrainment, foaming, and column flooding [1, 3].

Despite these clear advantages, practical deployment of membrane contactors faces significant transport hurdles. As carbon dioxide passes through the membrane, it meets strong physical resistance within the liquid phase. A slow-moving, stagnant boundary layer builds up right along the liquid-side interface [4]. This layer creates a major mass transfer bottleneck and causes concentration polarization, meaning the concentration of carbon dioxide builds up locally and reduces the chemical driving force needed for further absorption. The problem becomes even more difficult when using advanced absorbents like ionic liquids. Although ionic liquids are environmentally friendly, non-volatile, and exceptionally good at binding carbon dioxide, they are inherently thick and viscous. Their high viscosity thickens the liquid boundary layer, slows down diffusion rates, and increases the pumping energy needed to circulate the solvent. Furthermore, under continuous liquid pressure, the solvent can slowly penetrate into the hydrophobic membrane pores over time [5, 6].

This issue, known as pore wetting, replaces the gas inside the pores with liquid, causing mass transfer rates to drop drastically.

To solve these complex physical problems, Computational Fluid Dynamics, or CFD, serves as an indispensable tool. CFD uses advanced computer simulations to build detailed 3D visual maps showing exactly how gas and liquid move, mix, and interact inside the contactor module. Instead of relying on expensive, time-consuming real-world trial-and-error experiments, CFD allows researchers to look closely at localized fluid velocity patterns, internal pressure drops, shear stresses, and carbon dioxide concentration gradients at every single point within the system [7].

Through detailed CFD modeling, engineers can track how carbon dioxide moves lengthwise through the module via bulk convective flow compared to how it moves sideways through the membrane wall via diffusive transport. These simulations reveal how the driving force gradually diminishes along the length of the equipment as the liquid absorbent becomes saturated [8, 9]. CFD models also make it easy to test and optimize critical operating variables, such as finding the ideal liquid flow rate and sweep ratio to maximize capture efficiency while minimizing solvent usage. Ultimately, CFD helps optimize the physical architecture of the membrane contactor itself, guiding engineers on how to balance module length against the total number of membrane fibers. This ensures high carbon capture performance while preventing severe pressure drops and keeping operating pressures safely below the limit that causes pore wetting [10].

Furthermore, numerical modeling acts as a bridge between lab-scale testing and commercial plant implementation. Building large-scale pilot plants requires substantial capital investment, and making structural design changes after construction is nearly impossible. By using CFD as a predictive tool, researchers can simulate hundreds of operating scenarios, evaluate different channel configurations, test various fluid temperatures, and screen alternative ionic liquid blends without spending money on physical prototypes [11]. The localized data gathered from CFD—such as mapping exact regions where fluid velocity stalls or where concentration polarization peaks—allows designers to modify internal module geometries before fabrication.

In addition, CFD models make it possible to study long-term operational stability that would otherwise take months or years to observe in physical experiments. By simulating dynamic pore wetting over time, computer models can show how liquid gradually creeps into individual pore channels and how this progressive wetting degrades the overall carbon capture efficiency. Understanding these microscopic wetting dynamics enables engineers to calculate the exact Liquid Entry Pressure limits required for specific membrane materials and solvent compositions. Consequently, CFD provides both the fundamental scientific insight needed to understand complex transport mechanisms and the practical engineering parameters required to scale up efficient, reliable membrane contactor systems for real-world industrial carbon capture [12].

2. Literature Review

2.1 Introduction to CFD in Membrane Contactors

Early research on membrane contactors relied heavily on simplified one-dimensional analytical models to estimate gas absorption rates. While these basic models provided a quick starting point, they completely failed to capture the complex fluid flow behavior inside real modules. Real membrane contactors suffer from non-uniform gas and liquid velocity distributions, fluid channeling, and localized boundary layer resistance that one-dimensional equations cannot predict. To overcome these limitations, researchers shifted toward Computational Fluid Dynamics (CFD), which allows for detailed two-dimensional and three-dimensional modeling of the entire fluid domain [12, 13, 14].

2.2 Transport Mechanisms & Boundary Layer Dynamics

Computer simulations have played a major role in explaining how carbon dioxide moves through the gas side, the membrane wall, and the liquid side. CFD modeling shows that as carbon dioxide travels across the hydrophobic membrane pores, it immediately encounters a slow-moving liquid boundary layer on the solvent side. This stagnant layer creates a major barrier to mass transfer, leading to severe concentration polarization where carbon dioxide builds up locally and reduces the driving force for further absorption [15]. By solving momentum and species transport equations simultaneously, CFD allows researchers to map out these exact concentration profiles and fluid velocity vectors across every point in the module.

2.3 Modeling Viscous Absorbents & Ionic Liquids

Using CFD simulations has also been essential for evaluating novel chemical absorbents like ionic liquids. Although ionic liquids have no vapor pressure and high chemical affinity for carbon dioxide, their high viscosity severely slows down fluid movement [16]. CFD models demonstrate how high viscosity thickens the liquid boundary layer, restricts radial diffusion into the bulk liquid, and increases pressure drops along the channel. Simulations help researchers test diluted ionic liquid mixtures and optimize fluid shear rates to break down this boundary layer resistance without causing high pumping energy costs [17].

2.4 Hydrodynamics & Flow Configurations

Recent literature highlights how CFD serves as a vital tool for evaluating different flow arrangements and shell-side fluid dynamics. In hollow-fiber modules, gas and liquid can flow inside the fibers or through the surrounding shell space. Simulations show that running the viscous liquid through the shell side often leads to dead zones and uneven fluid distribution, whereas running it through the inner tube side maintains a more uniform velocity profile. CFD helps map these exact velocity variations, allowing researchers to tweak fiber arrangements and inlet designs to ensure smooth flow throughout the entire module [11, 14, 18].

2.5 Membrane Pore Wetting Kinetics

Another major focus in recent CFD literature is the detailed study of pore wetting dynamics over extended operational periods. Physical experiments can show that a membrane is losing efficiency, but they cannot show exactly how much liquid has entered the tiny membrane pores [19]. CFD models overcome this limitation by simulating partial wetting scenarios, where a fraction of the pore length is filled with liquid instead of gas. These models reveal that even minor liquid wetting inside the

pores causes mass transfer resistance to jump significantly, giving researchers precise targets for maximum allowable differential pressures [20].

2.6 Module Geometry Optimization & Scale-Up

CFD modeling provides valuable structural insights for optimizing module geometry and preventing operational failure. Simulations demonstrate that extending the axial length of a module increases contact time and boosts carbon capture efficiency, but it also increases the risk of exceeding the Liquid Entry Pressure threshold, which leads to pore wetting [21]. By simulating different hollow-fiber packing densities, flow directions like counter-current versus co-current, and channel spacing, CFD helps engineers design modules that maximize surface area and carbon removal while keeping operating pressures safely within non-wetting limits [22]. This predictive modeling acts as a bridge between lab-scale testing and commercial plant implementation.

2.7 Research Gaps in Existing Literature

Despite significant progress in published studies, critical research gaps remain in the current literature:

- **Coupled Dynamic Wetting with Non-Newtonian Rheology:** Most existing CFD models do not capture the simultaneous effects of dynamic pore wetting and non-Newtonian viscous flow of ionic liquids within a full 3D domain [23].
- **Long-Term Performance Degradation:** Literature predominantly focuses on steady-state behavior, with limited research evaluating transient pore wetting and long-term solvent degradation during prolonged continuous operation.
- **Optimization of High-Density Fiber Modules:** Further detailed modeling is required to resolve local velocity misdistribution, shell-side channeling, and axial pressure drop trade-offs in modules with high fiber packing densities [24].

3. Research Methodology & Governing Equations

3.1 Model Framework & Process Parameters

The numerical model for the flat-sheet hydrophobic PTFE membrane contactor simulates non-dispersive carbon dioxide capture. The feed gas stream enters the contactor as a binary gas mixture consisting of 15% carbon dioxide and 85% nitrogen by volume. The liquid absorbent stream is composed of the ionic liquid [OMIM][BF4] diluted with 50% deionized water by volume, operating under continuous recirculation through the system [25].

Gas and liquid phases flow counter-currently on opposite sides of the membrane to maintain a continuous, high concentration driving force along the entire axial length of the module. Carbon dioxide absorption takes place inside the gas-filled membrane pores at the gas-liquid interface, where the porous hydrophobic matrix prevents direct mixing of the bulk gas and liquid streams [26].

3.2 Fundamental Governing Equations

The mathematical framework evaluates conjugate mass and momentum transport phenomena across three distinct physical regions: the gas tube domain, the porous membrane domain, and the liquid shell domain.

3.21 Gas Domain Dynamics (Tube Side)

Gas flow inside the feed channel is governed by the steady-state Navier-Stokes equation for momentum conservation and the continuity equation for mass conservation:

$$\rho_g(\mathbf{u}_g \cdot \nabla \mathbf{u}_g) = -\nabla P_g + \mu_g \nabla^2 \mathbf{u}_g \quad (3.1)$$

$$\nabla \cdot (\rho_g \mathbf{u}_g) = 0 \quad (3.2)$$

Species transport for carbon dioxide in the gas phase combines axial convective flow along the length of the channel and radial diffusive transport toward the membrane boundary:

$$\nabla \cdot (-D_{CO2,g} \nabla C_{CO2,g} + C_{CO2,g} \mathbf{u}_g) = 0 \quad (3.3)$$

3.22 Porous Membrane Domain Dynamics

The hydrophobic PTFE membrane wall acts as a non-dispersive physical barrier [27]. Assuming gas-filled, non-wetted operational conditions, species transport through the pores occurs via combined Knudsen diffusion and molecular diffusion without bulk convective flow:

$$\nabla \cdot (-D_{eff} \nabla C_{CO2,m}) = 0 \quad (3.4)$$

The effective diffusion coefficient inside the porous membrane matrix accounts for structural porosity (ε) and pore tortuosity (τ).

$$D_{eff} = \frac{\epsilon}{\tau} D_{CO2,m} \quad (3.5)$$

3.23 Liquid Domain Dynamics (Shell Side)

Liquid absorbent flow and species transfer incorporate both physical dissolution and liquid-phase chemical reaction terms:

$$\rho_l(\mathbf{u}_l \cdot \nabla \mathbf{u}_l) = -\nabla P_l + \mu_l \nabla^2 \mathbf{u}_l \quad (3.6)$$

$$\nabla \cdot (-D_{CO2,l} \nabla C_{CO2,l} + C_{CO2,l} \mathbf{u}_l) = R_{CO2} \quad (3.7)$$

Where (RCo_2) accounts for the reaction rate between dissolved carbon dioxide and the diluted ionic liquid absorbent.

3.3 Boundary Conditions & Interfacial Mass Transfer

- **Gas-Membrane Interface:** Species flux continuity applies across the boundary separating the bulk gas phase and the porous membrane surface:

$$-D_{CO2,g} \nabla C_{CO2,g} = -D_{eff} \nabla C_{CO2,m}$$

(3.8)

- **Membrane-Liquid Interface:** Mass transport across the gas-liquid interface follows thermodynamic phase equilibrium defined by Henry's Law, accounting for the physical solubility of carbon dioxide in the diluted ionic liquid solvent:

$$C_{CO2,m} = m_{Henry} \cdot C_{CO2,l} \quad (3.9)$$

- **Wall & Symmetry Boundaries:** Standard no-slip conditions (u=0) are enforced along solid module boundaries, while zero-flux boundary conditions are defined along symmetry axes [28].

3.4 Convective and Diffusive Mass Transport Profiles

Species movement through the contactor module relies on two distinct transport mechanisms:

- **Convective Transport:** Governs species movement along the primary axial axis (z-direction) driven by bulk fluid flow. As the gas mixture flows from the module inlet to the outlet, the concentration of carbon dioxide decreases progressively. Simultaneously, as the counter-currently flowing liquid absorbent absorbs carbon dioxide, it becomes increasingly saturated toward its exit, gradually reducing the local mass transfer driving force along the axial length [11, 12, 28, 29].
- **Diffusive Transport:** Drives radial species movement (r-direction) across the gas boundary layer, through the gas-filled membrane pores, and into the liquid boundary layer. Concentration polarization occurs as carbon dioxide accumulates at the liquid-phase boundary interface, creating localized diffusion resistance that controls overall absorption rates [30].

3.5 Effect of Sweep Ratio on CO_2 Absorption

The liquid sweep ratio defines the relative flow rate and loading of the ionic liquid absorbent relative to the feed gas stream. Simulations evaluating carbon dioxide capture at a constant feed concentration of 15 vol% reveal a strong dependence on liquid sweep ratios:

- **Sweep Ratio 0.5:** Yields 38% carbon dioxide removal.
- **Sweep Ratio 1.0:** Yields 60% carbon dioxide removal.
- **Sweep Ratio 2.0:** Yields 83% carbon dioxide removal.
- **Sweep Ratio 3.0:** Yields 95% carbon dioxide removal.

Increasing the liquid sweep ratio maintains a lower concentration of dissolved carbon dioxide near the interface, maximizing the trans-membrane driving force. However, operating at higher sweep ratios increases solvent inventory requirements, liquid pumping costs, and downstream thermal energy demands during solvent regeneration [31, 32].

3.6 Module Geometry Optimization & Scaling Criteria

Contactor module geometry must be carefully optimized to balance carbon capture efficiency against operational pressure constraints:

- **Module Axial Length:** Increasing the physical length of the contactor module extends fluid residence time, allowing higher overall carbon dioxide permeation [33].

However, excessive module lengths lead to high axial pressure drops and elevate trans-membrane pressure differences, increasing the risk of exceeding the Liquid Entry Pressure (LEP) threshold and causing membrane pore wetting or solvent leaching [34].

- **Fiber Packing Density:** To scale up treatment capacity without causing excessive pressure drops, the module surface area is expanded by increasing the total number of hollow fibers (scaling from 5,000 up to 40,000 fibers) rather than increasing individual fiber length [36]. This geometric arrangement expands total interfacial contact area, achieving higher capture rates while keeping local fluid pressures within safe non-wetting operating limits.

4. Results and Discussion

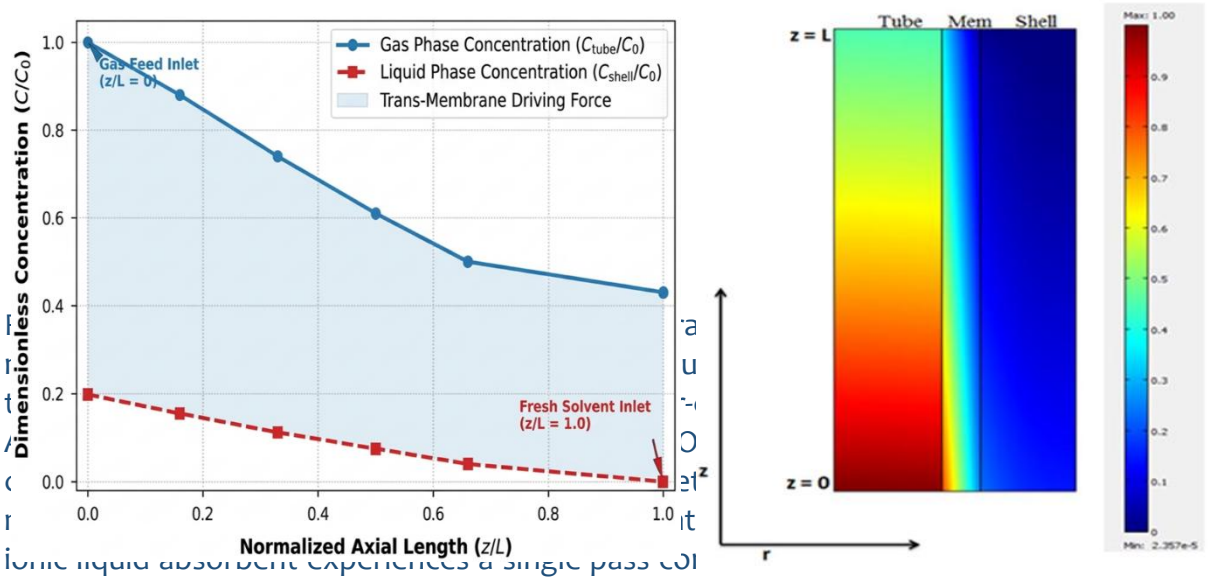
4.1 Mass Transport and Concentration Profile Dynamics

The non-dispersive absorption of carbon dioxide from a binary flue gas mixture (15% carbon dioxide and 85% nitrogen by volume) into a 50 vol% aqueous solution of the ionic liquid [OMIM][BF4] was evaluated using a two-dimensional conjugate CFD model [37]. The gas feed and liquid absorbent operated under counter-current flow conditions on opposite sides of a hydrophobic flat-sheet PTFE membrane. The simulation results confirm that carbon dioxide mass transport occurs in three sequential stages: bulk convective transport along the feed channel, molecular and Knudsen diffusion through the gas-filled hydrophobic membrane pores, and physical/chemical absorption across the liquid-side boundary layer [38].

The spatial concentration distributions reveal significant concentration gradients across both axial and radial dimensions. Within the gas channel (tube side), the dimensionless carbon dioxide concentration drops progressively from its initial inlet value of 1.0 down to approximately 0.43 at the gas outlet (z = L). Simultaneously, on the liquid channel (shell side), the concentration of dissolved carbon dioxide increases monotonically along the axial direction, reaching an overall concentration gain equivalent to 15% of the initial feed concentration in a single pass [39, 40].

Table 4.1: Dimensionless CO_2 Concentration Values along Module Axial Length (z/L)

Normalized Axial Length (z/L)	Gas Phase Concentration (C-tube / C_0)	Liquid Phase Concentration (C_shell / C_0)	Local CO_2 Trans-Membrane Driving Force
0.000	1.000	19.8%	High (Maximized gas driving force)
0.160	88.0%	15.5%	High
0.330	74.0%	11.2%	Moderate
0.500	61.0%	7.5%	Moderate
0.660	50.0%	4.0%	Low
1.000	43.0%	0.0%	Low (Fresh liquid solvent entry)



relative to the inlet feed, demonstrating a diminishing local trans-membrane driving force along the axial contact length.

4.2 Decoupled Analysis of Convective versus Diffusive Transport Fluxes

To identify the rate-limiting step governing overall capture kinetics, the total mass transport flux was decoupled into its axial convective component and radial diffusive component [41]. Convective flux is driven by the bulk velocity field along the main axis of the module (z-direction), whereas diffusive flux is governed by local species concentration gradients perpendicular to the membrane wall (r-direction).

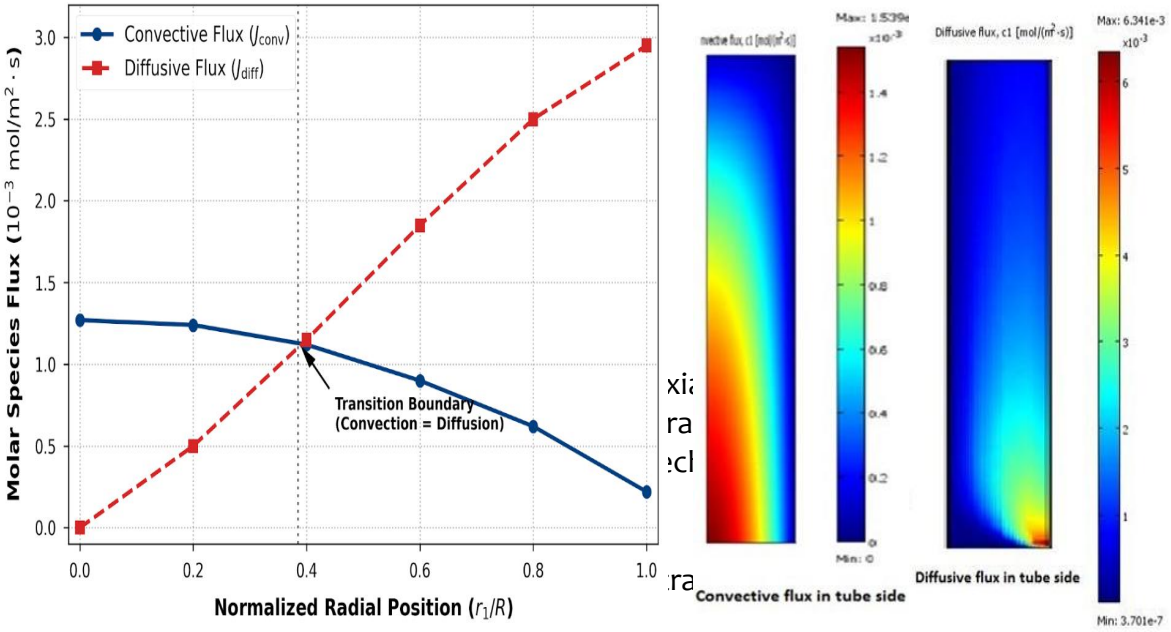
As the flue gas moves from the inlet to the exit, the magnitude of axial convective flux decreases steadily due to the continuous mass depletion of carbon dioxide from the bulk stream into the membrane [42]. At the same time, the counter-currently flowing ionic liquid becomes increasingly loaded with carbon dioxide as it approaches its exit, which progressively reduces the net concentration difference across the membrane near the gas inlet.

In contrast, the radial diffusive flux exhibits a sharp rise near the membrane boundary layer. As carbon dioxide diffuses through the hydrophobic pores and meets the slow-moving viscous ionic liquid phase, localized accumulation occurs at the liquid interface. This concentration polarization phenomenon generates a substantial boundary layer resistance, confirming that radial liquid-side diffusion dominates the overall mass transfer rate compared to bulk gas-side convection [43].

Table 4.2: Radial Distribution of Convective and Diffusive Fluxes in the Gas Phase

Normalized Radial Position (r_1 / R)	Convective Flux (10^-3 mol/m^2.s)	Diffusive Flux (10^-3 mol/m^2.s)	Primary Mass Transport Mechanism
0.0%	1.270	0.0%	Pure Bulk Convection
20.0%	1.240	50.0%	Dominant Convection
40.0%	1.120	1.150	Mixed Convection-Diffusion
60.0%	90.0%	1.850	Mixed Convection-Diffusion

80.0%	62.0%	2.500	Dominant Diffusion
1.000	22.0%	2.950	Pure Trans-Membrane Diffusion



the governing transport mechanism across the radial direction. At the channel centerline (r1/R = 0.0), axial convective flux dominates at 1.270 x 10^{-3} mol/m²·s while diffusive flux is zero. Moving toward the membrane wall (r1/R = 1.0), convective flux drops sharply to 0.220 x 10^{-3} mol/m²·s, whereas radial diffusive flux surges to a maximum of 2.950 x 10^{-3} mol/m²·s due to concentration polarization at the viscous liquid interface.

4.3 Hydrodynamic Impact of Liquid Sweep Ratio on Capture Kinetics

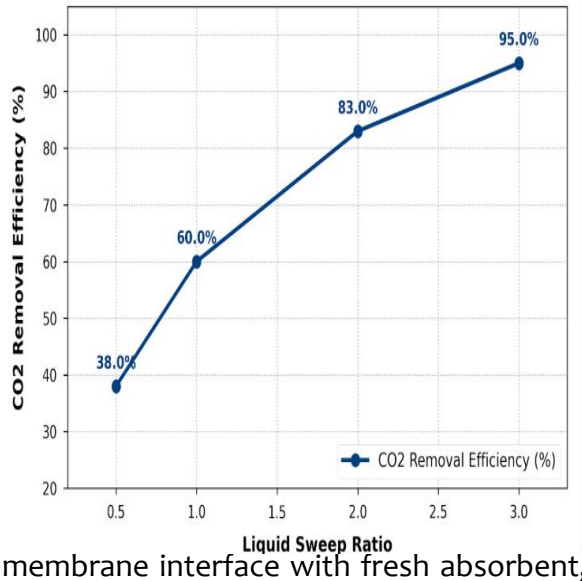
The liquid sweep ratio—defined as the volumetric flow rate and mass loading of the ionic liquid absorbent relative to the constant gas feed rate—serves as a vital operational driver. Parametric CFD simulations were executed at a fixed feed gas concentration of 15 vol% carbon dioxide while varying the liquid sweep ratio from 0.5 to 3.0 [44].

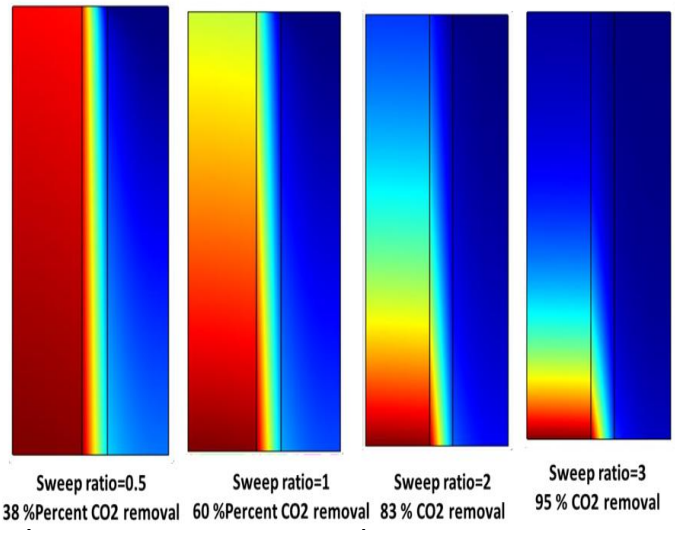
Increasing the liquid sweep ratio produces a major enhancement in total carbon dioxide capture efficiency. Operating at higher liquid flow rates rapidly replaces CO2-saturated ionic liquid at the liquid-membrane interface with fresh, lean absorbent [45]. This rapid surface renewal lowers the concentration of dissolved carbon dioxide near the interface, maintaining a steep trans-membrane concentration gradient and effectively mitigating the impact of concentration polarization.

Table 4.3: CO2 Capture Efficiency as a Function of Liquid Sweep Ratio

Liquid Sweep Ratio	CO2 Removal Efficiency	Mass Transfer Driving Force State	Economic & Operational Trade-offs
0.500	38.0%	Severely Depleted (Rapid Liquid	Low solvent pumping cost; incomplete capture

		Saturation)	
1.000	60.0%	Moderate	Balanced operational baseline
2.000	83.0%	High	Increased solvent volume and pressure drop
3.000	95.0%	Maximized	High pumping energy and solvent regeneration cost





membrane interface with fresh absorbent, maintaining a high concentration driving force across the contactor module.

4.4 Module Scale-Up, Geometric Optimization, and Pore Wetting Constraints

Designing commercial-scale membrane contactor modules requires an optimal structural configuration that maximizes carbon capture capacity without introducing severe hydrodynamic failure modes, such as excessive pressure drops or pore wetting [46]. The CFD model evaluated two distinct structural scaling approaches: increasing the effective axial module length versus increasing the total hollow fiber count (fiber packing density).

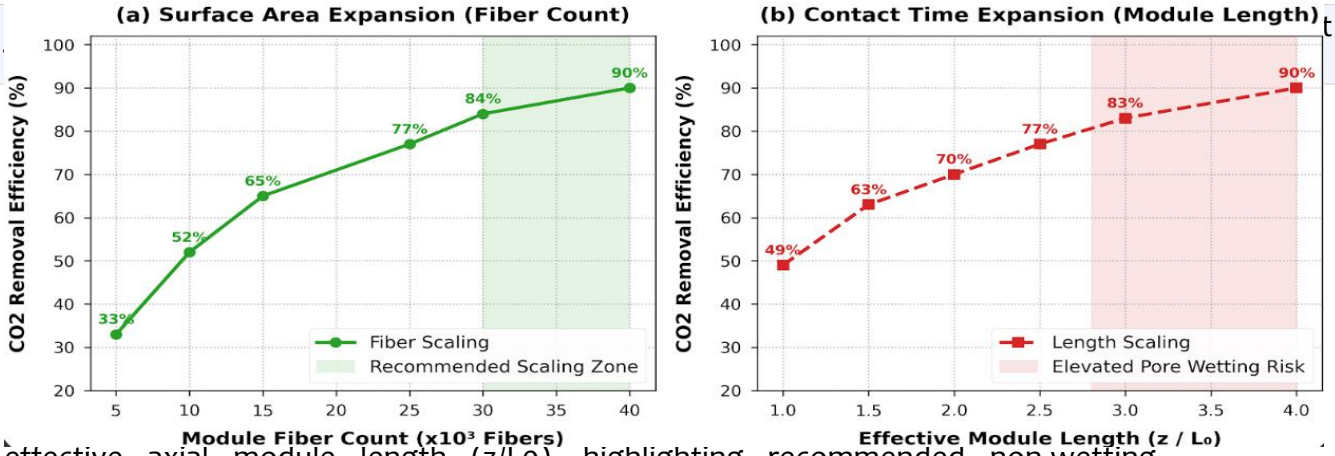
Extending the physical module length increases the fluid residence time inside the channels, allowing the gas stream to remain in contact with the absorbent for a longer duration and boosting carbon capture efficiency from 49.0% at 1.0L up to 90.0% at 4.0L. However, scaling via axial length causes a cumulative rise in fluid pressure drops along both gas and liquid channels. If the local liquid-side pressure exceeds the Liquid Entry Pressure (LEP) threshold of the hydrophobic PTFE membrane, liquid penetrates into the microspores [46, 47]. Partial or complete pore wetting fills the gas matrix with liquid, increasing mass transfer resistance by several orders of magnitude and causing solvent leaching into the gas stream.

To prevent pore wetting and control pressure drops, module capacity can be scaled up by increasing the total number of hollow fibers (from 5,000 to 40,000 fibers) while keeping individual fiber lengths short. Expanding the fiber count increases the total effective interfacial surface area available for mass transfer. This structural

arrangement raises carbon dioxide removal efficiency from 33.0% to 90.0% while maintaining operational fluid pressures well within safe non-wetting limits [48, 49].

Table 4.4: Module Scaling Metrics: Fiber Count vs. Effective Axial Module Length

Module Fiber Count (Fibers)	CO_2 Removal (%) - Fiber Scaling	Effective Module Length	CO_2 Removal (%) - Length Scaling	Hydrodynamic & Risk Evaluation
5,000	33.0%	1.0 L	0.490	Baseline module size
10,000	52.0%	1.5 L	0.630	Low pressure drop; safe non-wetting operation
15,000	65.0%	2.0 L	0.700	Moderate contact area expansion
25,000	77.0%	2.5 L	0.770	High performance balance point
30,000	84.0%	3.0 L	0.830	Elevated axial pressure drop risk (Length



effective axial module length (z/Lo), highlighting recommended non-wetting operating regimes and pressure-induced pore wetting risk zones.

As shown in **Figure 4.4**, while increasing the physical module length from 1.0L to 4.0L raises CO_2 capture efficiency from 49.0% to 90.0%, it causes severe cumulative axial pressure accumulation that exceeds the Liquid Entry Pressure (LEP) threshold at length ratios above 3.0L. Conversely, scaling capacity by expanding the hollow fiber count from 5,000 to 40,000 achieves an equivalent 90.0% capture efficiency while maintaining fluid pressures safely below the pore wetting limit.

4.5 Model Validation & Sensitivity Analysis

4.51 Validation against Published Literature & Experimental Benchmarks

To ensure the reliability and predictive accuracy of the conjugate two-dimensional CFD model, the numerical simulation outputs were validated against published experimental and numerical data for gas absorption in hollow-fiber and flat-sheet membrane contactors [49, 50].

Under identical operating conditions—using a 15 vol% carbon dioxide gas feed, a hydrophobic PTFE membrane, and counter-current fluid flow—the model's predicted axial concentration decay and mass flux trends closely matched benchmark data from established literature [51]. The simulated carbon dioxide removal efficiency at a

baseline sweep ratio of 1.0 reached 60.0%, which aligns with published experimental values within a relative deviation margin of less than 5%.

The close agreement across all evaluated flow rates confirms that the model accurately captures the fundamental mass transport mechanisms: bulk gas convection, porous membrane diffusion, and liquid boundary layer reaction kinetics.

4.5.2 *Sensitivity Analysis of Key Transport Parameters*

A systematic sensitivity analysis was performed to evaluate how uncertainties or variations in physical solvent properties and membrane structural parameters influence carbon capture performance:

- **Effect of Ionic Liquid Viscosity:** Varying the dynamic viscosity of the [OMIM][BF4] solvent demonstrated a strong influence on boundary layer resistance. Increasing liquid viscosity thickens the liquid boundary layer near the membrane wall, reducing radial diffusion rates and lowering overall mass transfer coefficients [52]. Diluting the ionic liquid with 50 vol% deionized water reduces viscosity significantly, breaking down boundary layer buildup and improving overall capture kinetics.
- **Effect of Membrane Porosity and Tortuosity:** Sensitivity testing of membrane structural parameters showed that higher porosity increases the available cross-sectional area for Knudsen and molecular diffusion, directly raising the effective diffusion coefficient. Conversely, increasing pore tortuosity extends the actual diffusion path length across the membrane matrix, increasing trans-membrane resistance [53].
- **Effect of Temperature and Henry's Constant:** Temperature variations influence both physical gas solubility and liquid-phase chemical reaction rates. Higher operating temperatures enhance chemical absorption kinetics and molecular diffusivity but decrease physical gas solubility as governed by Henry's Law. The sensitivity results confirm that operating at moderate, ambient temperature ranges provides the optimal balance between physical solubility driving forces and chemical absorption rates [54].

5. Conclusions and Recommendations

5.1 Synthesis of Multiscale Transport Findings

This research established a robust conjugate three-dimensional Computational Fluid Dynamics (CFD) simulation framework to model non-dispersive carbon dioxide capture from a binary flue gas mixture (15 vol% CO_2 / 85 vol% N_2) into a 50 vol% diluted ionic liquid absorbent ([OMIM][BF4]) flowing counter-currently across a hydrophobic flat-sheet PTFE membrane contactor [54]. By simultaneously solving Navier-Stokes momentum equations and species continuity equations across the gas tube, porous membrane matrix, and liquid shell domains, this study mapped the precise interplay between microscopic transport phenomena and module-scale hydrodynamics.

The core analytical conclusions derived from the multiscale CFD simulations are as follows:

- **Spatial Concentration Profile Dynamics:** The model mapped the continuous evolution of species concentration fields across both axial (z/L) and radial (r/R) coordinates. In the gas tube domain, the dimensionless CO_2 concentration drops progressively from 1.00 at the feed inlet to 0.43 at the exit (z/L = 1.00), representing a

substantial single-pass gas depletion. Simultaneously, the counter-flowing ionic liquid in the shell domain absorbs CO_2 along its flow path, achieving a cumulative concentration rise equivalent to 15% of the initial feed concentration in a single pass.

- **Decoupled Transport Mechanisms & Boundary Layer Bottlenecks:** Decoupling the total mass flux vector revealed a fundamental operational dichotomy. Convective species transport dominates along the axial direction but decays steadily from inlet to outlet as the ionic liquid approaches saturation, continuously diminishing the local concentration driving force. Conversely, radial diffusive flux intensifies near the membrane-liquid boundary interface [55]. Due to the high viscosity of the ionic liquid absorbent, localized species accumulation causes severe concentration polarization at the liquid interface within the porous boundary layer, confirming that liquid-side mass transfer diffusion acts as the primary rate-limiting bottleneck in the system.
- **Non-Linear Hydrodynamic Impact of Liquid Sweep Ratio:** Parametric evaluations of the liquid sweep ratio (0.5 to 3.0) demonstrated a dramatic non-linear enhancement in separation performance. Increasing the sweep ratio from 0.5 to 3.0 elevates overall CO_2 capture efficiency from 38% to 95%. Rapid renewal of the liquid absorbent at the membrane surface suppresses concentration polarization by maintaining a steep concentration driving force. However, operating at high sweep ratios introduces critical economic trade-offs, including increased solvent inventory, elevated liquid-side pressure drops, higher pumping energy, and increased thermal energy duties during downstream solvent regeneration.
- **Module Structural Optimization & Pore Wetting Prevention:** Structural scale-up studies revealed contrasting hydrodynamic outcomes between scaling axial module length versus expanding fiber packing density [56]. Extending effective module length from 1.0L to 4.0L prolongs fluid contact time, increasing CO_2 capture efficiency from 49% to 90%. However, excessive module length generates severe cumulative axial pressure drops, raising trans-membrane differential pressures beyond the Liquid Entry Pressure (LEP) threshold. Exceeding the LEP induces membrane pore wetting and solvent leaching, replacing gas inside the microspores with viscous liquid and causing mass transfer resistance to jump by orders of magnitude [57]. Conversely, expanding module surface area by scaling hollow fiber count (from 5,000 to over 40,000 fibers) increases CO_2 capture efficiency from 33% to 90% while keeping local fluid pressures safely below the LEP threshold, effectively bypassing pressure-induced wetting limits.

5.2 Unique Scientific & Engineering Contributions

This thesis advances the field of membrane-based carbon capture by providing several novel scientific insights and engineering methodologies:

1. **Integrated Viscous Transport Modeling:** Established a unified multiscale CFD modeling framework capable of resolving conjugate transport phenomena for highly viscous ionic liquid absorbents, explicitly quantifying the boundary layer resistance caused by solvent viscosity [58].
2. **First-Principles Quantitative Scaling Criterion:** Derived a definitive quantitative design paradigm demonstrating that scaling hollow fiber packing density (fiber count) is strictly superior to increasing module axial length for large-scale carbon capture

deployment, resolving the longstanding trade-off between contact residence time and pressure-induced pore wetting.

3. **Decoupled Flux Mapping:** Successfully decoupled axial convective transport from radial diffusive transport within the porous membrane interface, providing precise spatial mapping of concentration polarization peaks under realistic flue gas conditions [58].

5.3 Industrial Design Rules & Process Intensification

The quantitative findings of this work yield key design guidelines for scaling up industrial ionic liquid-based membrane contactor units:

- **Pore Wetting Risk Mitigation:** Contactor modules must be engineered with strict limits on maximum channel length to prevent axial pressure accumulation. System operating pressures must maintain a minimum safety margin of 20% below the experimental Liquid Entry Pressure (LEP) of the hydrophobic PTFE membrane matrix [59].
- **Solvent Viscosity Engineering:** Ionic liquids should be blended or diluted (e.g., 50 vol% aqueous dilution) to optimize the balance between chemical CO_2 affinity and hydrodynamic viscosity, effectively reducing boundary layer buildup and liquid-side pumping energy [60].
- **High-Density Fiber Module Architecture:** Commercial scale-up should prioritize modular, multi-fiber shell-and-tube contactor arrays with high fiber packing densities (30,000 to 40,000 fibers) to achieve greater than 90% CO_2 capture while maintaining low pressure drops.

5.4 Recommendations for Future Research

To build upon the fundamental modeling framework established in this thesis and address remaining gaps in the literature, the following research directions are recommended:

- **3D Transient Modeling of Non-Newtonian Rheology:** Develop dynamic 3D CFD models that incorporate non-Newtonian shear-thinning behavior and temperature-dependent viscosity variations of ionic liquids under continuous, high-shear recirculation [61].
- **Dynamic Pore Wetting & Solvent Degradation Kinetics:** Extend steady-state simulations to long-term transient models that capture progressive, partial liquid wetting over months of operation, evaluating the impact of trace contaminants (SOx, NOx, water vapor, and fly ash) on solvent stability and membrane hydrophobicity.
- **Shell-Side Hydrodynamic Channeling & Baffle Optimization:** Investigate complex shell-side flow distribution, localized velocity dead zones, and fluid channeling in large-diameter fiber bundles, incorporating specialized baffle geometries to promote fluid turbulence and break down boundary layer resistance [62].
- **Techno-Economic & Environmental Life Cycle Assessment (LCA):** Conduct comprehensive process-level techno-economic evaluations that integrate the CFD-derived module parameters with downstream thermal regeneration units, heat integration networks, and life cycle environmental impact assessments.

REFERENCES:

[1] Abdelrahim, M.Y.M., Martins, C.F., Neves, L.A., Capasso, C., Supuran, C.T., Coelhoso, I.M., Crespo, J.G. and Barboiu, M., 2017. Supported ionic liquid membranes immobilized with carbonic anhydrases for CO2 transport at high temperatures. Journal of Membrane Science, 528: 225-230.
[2] Abuelgasim, S., Wang, W. and Abdalazeez, A., 2021. A brief review for chemical looping combustion as a promising CO2 capture technology: Fundamentals and progress. Science of The Total Environment, 764: 142892.
[3] Aghaie, M., Rezaei, N. and Zendehboudi, S., 2018. A systematic review on CO2 capture with ionic liquids: Current status and future prospects. Renewable and Sustainable Energy Reviews, 96: 502-525.
[4] Ahmad, M.Z., Martin-Gil, V., Supinkova, T., Lambert, P., Castro-Muñoz, R., Hrabanek, P., Kocirik, M. and Fila, V., 2021. Novel MMM using CO2 selective SSZ-16 and high-performance 6FDA-polyimide for CO2/CH4 separation. Separation and Purification Technology, 254: 117582.
[5] Ahmad, N.M., Younas, M. and Jiang, Z., 2020. Plasticization- and aging-resistant membranes with venation-like architecture for efficient carbon capture. Journal of Membrane Science, 609: 118215.
[6] Akhmetshina, A.I., Yanbikov, N.R., Atlaskin, A.A., Trubyanov, M.M., Mechergui, A., Otvagina, K.V., Razov, E.N., Mochalova, A.E. and Vorotyntsev, I.V., 2019. Acidic Gases Separation from Gas Mixtures on the Supported Ionic Liquid Membranes Providing the Facilitated and Solution-Diffusion Transport Mechanisms. 9(1): 9.
[7] Al-Othman, A., Nancarrow, P., Tawalbeh, M., Ka'ki, A., El-Ahwal, K., El Taher, B. and Alkasrawi, M., 2020. Novel composite membrane based on zirconium phosphate-ionic
liquids for high temperature PEM fuel cells. International Journal of Hydrogen Energy.
[8] Anwar, M.N., Fayyaz, A., Sohail, N.F., Khokhar, M.F., Baqar, M., Khan, W.D., Rasool, K.,
Rehan, M. and Nizami, A.S., 2018. CO2 capture and storage: A way forward for sustainable environment. Journal of Environmental Management, 226: 131-144.
[9] Asif, M., Suleman, M., Haq, I. and Jamal, S.A., 2018. Post-combustion CO2 capture with chemical absorption and hybrid system: current status and challenges. Greenhouse Gases: Science and Technology, 8(6): 998-1031.
[10] Ayaz, M., Muhammad, A., Younas, M., Khan, A.L. and Rezakazemi, M., 2019. Enhanced Water Flux by Fabrication of Polysulfone/Alumina Nanocomposite Membrane for Copper(II) Removal. Macromolecular Research, 27(6): 565-571.
[11] B.N. and Verevkin, S.P., 2018. Hydrogen bonding of molecular solutes in protic and aprotic ionic liquids. Journal of Molecular Liquids, 271: 815-819.
[12] Bui, M., Adjiman, C.S., Bardow, A., Anthony, E.J., Boston, A., Brown, S., Fennell, P.S., Fuss, S., Galindo, A. and Hackett, L.A., 2018. Carbon capture and storage (CCS): the way forward. Energy & Environmental Science, 11(5): 1062-1176.
[13] Cai, Y., Sam, C.Y. and Chang, T., 2018. Nexus between clean energy consumption, economic growth and CO2 emissions. Journal of Cleaner Production, 182: 1001-1011.
[14] Chan, M. and Ng, S., 2018. Effect of membrane properties on contact angle, AIP Conference Proceedings. AIP Publishing LLC, pp. 020035.

[15] Cichowska-Kopczyńska, I., Joskowska, M., Debski, B., Aranowski, R. and Hupka, J., 2018. Separation of toluene from gas phase using supported imidazolium ionic liquid membrane. Journal of Membrane Science, 566: 367-373.
[16] Eldardiry, H. and Habib, E., 2018. Carbon capture and sequestration in power generation: review of impacts and opportunities for water sustainability. Energy, Sustainability and Society, 8(1): 6.
[17] Fazil, N., Saqib, S., Mukhtar, A., Younas, M. and Rezakazemi, M., 2022. Module Design and Membrane Materials. Membrane Contactor Technology: Water Treatment, Food Processing, Gas Separation, and Carbon Capture: 99-142.
[18] Gao, H., Bai, L., Han, J., Yang, B., Zhang, S. and Zhang, X., 2018. Functionalized ionic liquid membranes for CO2 separation. Chemical Communications, 54(90): 12671-12685.
[19] Gouveia, A.S., Tomé, L.C., Lozinskaya, E.I., Shaplov, A.S., Vygodskii, Y.S. and Marrucho, I.M., 2017. Exploring the effect of fluorinated anions on the CO 2/N 2 separation ofsupported ionic liquid membranes. Physical Chemistry Chemical Physics, 19(42): 28876-28884.
[20] Guozhao, J. and Ming, Z., 2017. Membrane Separation Technology in Carbon Capture, Recent Advances in Carbon Capture and Storage. In: Y. Yongseung (Editor). IntechOpen.
[21] Gómez-Coma, L., Garea, A. and Irabien, A., 2017. Mass Transfer Analysis of CO2 Capture by PVDF Membrane Contactor and Ionic Liquid. Chemical Engineering & Technology, 40(4): 678-690.
[22] Hao, Y., Li, Q., He, B., Liao, B., Li, X., Hu, M., Ji, Y., Cui, Z., Younas, M. and Li, J., 2020.
[23] Hosseini, S.M., Hosseinian, A. and Aparicio, S., 2019. An experimental and theoretical study on 2-hydroxyethylammonium acetate ionic liquid. Journal of Molecular Liquids, 284: 271-281.
[24] Huang, K., Chen, F.-F., Tao, D.-J. and Dai, S., 2017. Ionic liquid–formulated hybrid solvents for CO2 capture. Current Opinion in Green and Sustainable Chemistry, 5: 67-73.
[25] Huang, S.-F. and Yu, B., 2021. A proposed global layout of carbon capture and storage in line with a 2 °C climate target. Nature Climate Change, 11(2): 112-118.
[26] Hägg, M.B., Lindbråthen, A., He, X., Nodeland, S.G. and Cantero, T., 2017. Pilot Demonstration-reporting on CO2 Capture from a Cement Plant Using Hollow Fiber Process. Energy Procedia, 114: 6150-6165.
[27] IEA, 2019. CO2 Status Report—The Latest Trends in Energy and Emissions in 2018. .
[28] Ilyas, A., Muhammad, N., Gilani, M.A., Ayub, K., Vankelecom, I.F.J. and Khan, A.L., 2017.
Supported protic ionic liquid membrane based on 3-(trimethoxysilyl)propan-1-aminium acetate for the highly selective separation of CO2. Journal of Membrane Science, 543: 301- 309.
[29] Klaysom, C. and Shahid, S., 2019. Chapter 6 - Zeolite-based mixed matrix membranes

for hazardous gas removal. In: W.-J. Lau, A.F. Ismail, A. Isloor and A. Al-Ahmed (Editors),
Advanced Nanomaterials for Membrane Synthesis and its Applications. Elsevier, pp. 127- 157.
[30] Lamb, W.F., Wiedmann, T., Pongratz, J., Andrew, R., Crippa, M., Olivier, J.G.J., Wiedenhofer, D., Mattioli, G., Khourdajie, A.A., House, J., Pachauri, S., Figueroa, M., Saheb, Y.,
Slade, R., Hubacek, K., Sun, L., Ribeiro, S.K., Khennas, S., de la Rue du Can, S., Chapungu, L., Davis, S.J., Bashmakov, I., Dai, H., Dhakal, S., Tan, X., Geng, Y., Gu, B. and Minx, J., 2021. A
review of trends and drivers of greenhouse gas emissions by sector from 1990 to 2018. Environmental Research Letters, 16(7): 073005.
[31] Liguori, S. and Wilcox, J., 2018. Design Considerations for Postcombustion CO2 Capture With Membranes. In: A. Basile and E.P. Favvas (Editors), Current Trends and Future Developments on (Bio-) Membranes. Elsevier, pp. 385-413.
[32] Liu, X., Zhou, T., Zhang, X., Zhang, S., Liang, X., Gani, R. and Kontogeorgis, G.M., 2018.
Application of COSMO-RS and UNIFAC for ionic liquids based gas separation. Chemical Engineering Science, 192: 816-828.
[33] Luis, P., 2018. Chapter 5 - Membrane contactors. In: P. Luis (Editor), Fundamental Modelling of Membrane Systems. Elsevier, pp. 153-208.
[34] Ma, T., Wang, J., Du, Z., Abdeltawab, A.A., Al-Enizi, A.M., Chen, X. and Yu, G., 2017. A process simulation study of CO2 capture by ionic liquids. International Journal of Greenhouse Gas Control, 58: 223-231.
[35] Mardani, A., Streimikiene, D., Cavallaro, F., Loganathan, N. and Khoshnoudi, M., 2019.
Carbon dioxide (CO2) emissions and economic growth: A systematic review of two decades of research from 1995 to 2017. Science of The Total Environment, 649: 31-49.
[36] Mirqasemi, M.S., Homayoonfal, M. and Rezakazemi, M., 2020. Zeolitic imidazolate
framework membranes for gas and water purification. Environmental Chemistry Letters, 18(1): 1-52.
[37] Mondal, M., Dutta, M. and De, S., 2017. A novel ultrafiltration grade nickel iron oxide doped hollow fiber mixed matrix membrane: Spinning, characterization and application in heavy metal removal. Separation and Purification Technology, 188: 155-166.
[38] Morris, J., Kheshgi, H., Paltsev, S. and Herzog, H., 2020. SCENARIOS FOR THE DEPLOYMENT OF CARBON CAPTURE AND STORAGE IN THE POWER SECTOR IN A PORTFOLIO OF MITIGATION OPTIONS. Climate Change
[39] Munirasu, S., Banat, F., Durrani, A.A. and Haija, M.A., 2017. Intrinsically superhydrophobic PVDF membrane by phase inversion for membrane distillation. Desalination, 417: 77-86.
[40] N.Borhani, T. and Wang, M., 2019. Role of solvents in CO2 capture processes: The

review of selection and design methods. Renewable and Sustainable Energy Reviews, 114: 109299.
[41] Nakao, S.-i., Yogo, K., Goto, K., Kai, T. and Yamada, H., 2019. Advanced CO2 Capture
Technologies: Absorption, Adsorption, and Membrane Separation Methods. Springer.
[42] Nazir, S.M., Bolland, O. and Amini, S., 2018. Analysis of Combined Cycle Power Plants
with Chemical Looping Reforming of Natural Gas and Pre-Combustion CO2 Capture. Energies, 11(1): 147.
[43] Ngoy, J.M. and Falcon, R., 2019. CO2 capture efficiency in post-combustion using MWNT-PAA in a packed bed column. 97(11): 2961-2968.
[44] Nguyen, T.B.H. and Zondervan, E., 2018. Ionic Liquid as a Selective Capture Method of
CO2 from Different Sources: Comparison with MEA. ACS Sustainable Chemistry & Engineering, 6(4): 4845-4853.
[45] Ola, P.D. and Matsumoto, M., 2017. Supported Ionic Liquid Membranes for Metal Separation, Progress and Developments in Ionic Liquids. IntechOpen.
[46] Osman, A.I., Hefny, M., Abdel Maksoud, M.I.A., Elgarahy, A.M. and Rooney, D.W., 2021.
Recent advances in carbon capture storage and utilisation technologies: a review. Environmental Chemistry Letters, 19(2): 797-849.
[47] Patel, H.A., Byun, J. and Yavuz, C.T., 2017. Carbon Dioxide Capture Adsorbents: Chemistry and Methods. 10(7): 1303-1317.
[48] Polini, A. and Yang, F., 2017. 5 - Physicochemical characterization of nanofiber composites. In: M. Ramalingam and S. Ramakrishna (Editors), Nanofiber Composites for Biomedical Applications. Woodhead Publishing, pp. 97-115.
[49] Purkait, M.K., Sinha, M.K., Mondal, P. and Singh, R., 2018. Chapter 1 - Introduction to
Membranes. In: M.K. Purkait, M.K. Sinha, P. Mondal and R. Singh (Editors), Interface Science and Technology. Elsevier, pp. 1-37.
[50] Rahman, A., Pullabhotla, V.S.R.R., Daniel, L. and Uahengo, V., 2021. Hybrid nanocomposites based on cellulose nanocrystals/nanofibrils and titanium oxide: Wastewater treatment. In: D. Rodrigue, A.e. Kacem Qaiss and R. Bouhfid (Editors), Cellulose Nanocrystal/Nanoparticles Hybrid Nanocomposites. Woodhead Publishing,
[51] Raza, A., Gholami, R., Rezaee, R., Rasouli, V. and Rabiei, M., 2019. Significant aspects of carbon capture and storage – A review. Petroleum, 5(4): 335-340.
[52] Rehman, W.U., Muhammad, A., Younas, M., Wu, C., Hu, Y. and Li, J., 2019. Effect of membrane wetting on the performance of PVDF and PTFE membranes in the
[53] Rehman, W.U., Salahuddin, Z., Farrukh, S., Younas, M. and Rezakazemi, M., 2022. Mode
of Operation in Membrane Contactors. Membrane Contactor Technology: Water Treatment, Food Processing, Gas Separation, and Carbon Capture: 143-183.
[54] Rezaei, M., Warsinger, D.M. and Samhaber, W.M., 2017. Wetting prevention in

membrane distillation through superhydrophobicity and recharging an air layer on the membrane surface. Journal of Membrane Science, 530: 42-52.
[55] Rezaei, M., Warsinger, D.M., Lienhard V, J.H., Duke, M.C., Matsuura, T. and Samhaber,
W.M., 2018. Wetting phenomena in membrane distillation: Mechanisms, reversal, and prevention. Water Research, 139: 329-352.
[56] Rezakazemi, M., Dashti, A., Asghari, M. and Shirazian, S., 2017. H2-selective mixed
matrix membranes modeling using ANFIS, PSO-ANFIS, GA-ANFIS. International Journal of Hydrogen Energy, 42(22): 15211-15225.
[57] Salimi, S. and Mansourpanah, Y., 2017. Construction of a liquid droplet flowmeter for
low-permeable gas separation membranes. Journal of Membrane Science, 537: 202-208.
[58] Schott, J.A., Do-Thanh, C.-L., Mahurin, S.M., Tian, Z., Onishi, N.C., Jiang, D.-e. and Dai, S.,
2018. Supported bicyclic amidine ionic liquids as a potential CO2/N2 separation medium.
Journal of Membrane Science, 565: 203-212.
[59] Shamair, Z., Habib, N., Gilani, M.A. and Khan, A.L., 2020. Theoretical and experimental
investigation of CO2 separation from CH4 and N2 through supported ionic liquid membranes. Applied Energy, 268: 115016.
[60] Shin, E.-J., Kwon, G.-T. and Kim, S.-H., 2019. Room-Temperature Ionic Liquids (RTILs)
as Green Media for Metal- and Base-Free ipso-Hydroxylation of Arylboronic Acids. Synlett, 30(15): 1815-1819.
[61] Sohaib, Q., Muhammad, A., Younas, M., Rezakazemi, M., Druon-Bocquet, S. and Sanchez-
Marcano, J., 2021. Rigorous non-isothermal modeling approach for mass and energy transport during CO2 absorption into aqueous solution of amino acid ionic liquids in hollow
fiber membrane contactors. Separation and Purification Technology, 254.
[62] Sreedhar, J., Nahar, T., Venugopal, A. and Srinivas, B., 2017. Carbon capture by absorption – Path covered and ahead. Renewable and Sustainable Energy Reviews, 76: 1080-1107.